The Astrophysical Journal, 855:27 (11pp), 2018 March 1 https://doi.org/10.3847/1538-4357/aaaa6a

Adsorption Energies of Carbon, Nitrogen, and Oxygen Atoms on the Low-temperature Amorphous Water Ice: A Systematic Estimation from Quantum Chemistry Calculations

Takashi Shimonishi[1,2,7], Naoki Nakatani[3,4,7], Kenji Furuya[5], and Tetsuya Hama[6]
[1] Frontier Research Institute for Interdisciplinary Sciences, Tohoku University, Aramakiazaaoba 6-3, Aoba-ku, Sendai, Miyagi, 980-8578, Japan; shimonishi@astr.tohoku.ac.jp
[2] Astronomical Institute, Tohoku University, Aramakiazaaoba 6-3, Aoba-ku, Sendai, Miyagi, 980-8578, Japan
[3] Institute for Catalysis, Hokkaido University, N21W10 Kita-ku, Sapporo, Hokkaido 001-0021, Japan; naokin@tmu.ac.jp
[4] Department of Chemistry, Graduate School of Science and Engineering, Tokyo Metropolitan University, 1-1 Minami-Osawa, Hachioji, Tokyo 192-0397, Japan
[5] Center for Computational Sciences, The University of Tsukuba, 1-1-1, Tennodai, Tsukuba, Ibaraki 305-8577, Japan
[6] Institute for Low Temperature Science, Hokkaido University, N19W8 Kita-ku, Sapporo, Hokkaido 060-0819, Japan
Received 2017 November 27; revised 2018 January 22; accepted 2018 January 22; published 2018 March 1

Abstract

We propose a new simple computational model to estimate the adsorption energies of atoms and molecules to low-temperature amorphous water ice, and we present the adsorption energies of carbon (^3P), nitrogen (^4S), and oxygen (^3P) atoms based on quantum chemistry calculations. The adsorption energies were estimated to be 14,100 ± 420 K for carbon, 400 ± 30 K for nitrogen, and 1440 ± 160 K for oxygen. The adsorption energy of oxygen is consistent with experimentally reported values. We found that the binding of a nitrogen atom is purely physisorption, while that of a carbon atom is chemisorption, in which a chemical bond to an O atom of a water molecule is formed. That of an oxygen atom has a dual character, with both physisorption and chemisorption. The chemisorption of atomic carbon also implies the possibility of further chemical reactions to produce molecules bearing a C–O bond, though this may hinder the formation of methane on water ice via sequential hydrogenation of carbon atoms. These properties would have a large impact on the chemical evolution of carbon species in interstellar environments. We also investigated the effects of newly calculated adsorption energies on the chemical compositions of cold dense molecular clouds with the aid of gas-ice astrochemical simulations. We found that abundances of major nitrogen-bearing molecules, such as N_2 and NH_3, are significantly altered by applying the calculated adsorption energy, because nitrogen atoms can thermally diffuse on surfaces, even at 10 K.

Key words: astrochemistry – ISM: abundances – ISM: atoms – ISM: molecules

1. Introduction

The formation of molecules on grain surfaces plays an essential role in the chemical evolution of cold and dense molecular clouds. Adsorption energy ($E_{\rm ads.}$) and diffusion activation energy ($E_{\rm diff.}$) of surface atoms and molecules are some of the important parameters that control the efficiency of grain surface reactions. Astrochemical simulations of gas-grain chemistry suggest that chemical compositions of dense molecular clouds are highly dependent on the $E_{\rm ads.}$ assumed in the simulation (Penteado et al. 2017; Wakelam et al. 2017). $E_{\rm diff.}$ can be estimated as a fraction of the $E_{\rm ads.}$ of surfaces species; the ratio of $E_{\rm diff.}$ to $E_{\rm ads.}$ often ranges from 0.3 to 1.0 (e.g., Sladek et al. 1974; Medveď & Černỳ 2011; Karssemeijer & Cuppen 2014; Cuppen et al. 2017). Accurate information on the adsorption energies of major surface species is thus crucial for astrochemical modeling of dense molecular cloud chemistry.

The values of $E_{\rm ads.}$ of stable molecules have been experimentally determined using thermal desorption spectroscopy such as temperature-programmed desorption (TPD) methods (e.g., Burke & Brown 2010; Hama & Watanabe 2013). However, TPD methods are not appropriate for reactive atoms (e.g., H) because they can barrierlessly recombine to form stable molecules on surfaces before thermal desorption (H + H → H_2). In addition, direct detection of atoms is difficult using quadrupole mass spectrometers with electron ionization. The $E_{\rm ads.}$ and $E_{\rm diff.}$ of atoms have been indirectly obtained from the analysis of TPD spectra of molecular products using a rate-equation model with $E_{\rm ads.}$ and $E_{\rm diff.}$ as parameters. However, the experimental results can be contradictory, depending on the difference in the experimental conditions (e.g., the incident flux of the atoms) and assumptions about the surface coverage of atoms (Manicò et al. 2001; Hornekaer et al. 2003; Pirronello et al. 2004; Perets et al. 2005; Vidali et al. 2006; Matar et al. 2008; Hama & Watanabe 2013).

To overcome this problem, the photo-stimulated desorption and resonance-enhanced multiphoton ionization (PSD-REMPI) method was developed to directly investigate adsorption and diffusion of H atoms on water ice (Watanabe et al. 2010; Hama et al. 2012; Kuwahata et al. 2015), but the PSD-REMPI method has yet to be applied to other atoms such as C, N, and O. Recent laboratory studies have suggested that the $E_{\rm ads.}$ of atomic oxygen (O) on interstellar dust analogs (1400–1700 K) significantly deviates from the traditionally adopted value of 800 K estimated by Tielens & Hagen (1982), on the basis of its polarizability (Ward et al. 2012; Kimber et al. 2014; He et al. 2015; Minissale et al. 2016). An experimental approach is also applied to the adsorption energy of atomic nitrogen in Minissale et al. (2016), while laboratory measurements for atomic carbon have not been reported so far. These experimental studies indicate the importance of revisiting the

[7] These authors contributed equally to this work.

$E_{ads.}$ of surface species with the aid of the latest computational techniques.

Theoretically estimating the adsorption energies of atoms and molecules on water ice is a still challenging work, even though we are able to use high-performance computers, because interstellar phenomena take at least thousands of years to complete, a timescale that is impossible to implement into the current computer resources. Therefore, a suitable computational model with reliable approximations is indispensable in practical simulations for interstellar chemistry.

Buch & Czerminski (1991), Al-Halabi et al. (2002), and Al-Halabi & van Dishoeck (2007) reported molecular dynamics simulations to theoretically investigate the collision process between a hydrogen atom and crystalline and amorphous water ice. They employed potential parameters that were generated from ab initio quantum chemical calculations. Many subsequent simulations extensively studied sticking probability, adsorption, and the diffusion of H atoms on water ice (e.g., Veeraghattam et al. 2014; Dupuy et al. 2016; Ásgeirsson et al. 2017; Senevirathne et al. 2017). The mobility of an O atom in amorphous ice at low temperatures was also recently studied using classical molecular dynamics (Lee & Meuwly 2014). However, classical molecular dynamics cannot capture chemical reaction because bond reformation is not involved in the computational models. Theoretical approaches based on quantum chemical calculations are thus highly desirable for understanding the adsorption of atoms, especially C, N, and O atoms, on water ice.

Quantum chemical calculations are now often used to theoretically investigate chemical reactions. For example, Ozkan & Dede (2012) reported a theoretical work on the chemical evolution of a carbon atom with a water molecule, based on ab initio quantum chemical calculations. They considered chemical reactions between singlet and triplet carbon atoms and one water molecule for the formation of a formaldehyde. Though they employed high-level quantum chemical theories to explore the chemical reactions, possibly due to computational limitations, their computational model involved only one water molecule, which is far from a realistic condition in interstellar ices.

Recently, Wakelam et al. (2017) also reported the binding energies of various atoms and molecules to one water molecule based on quantum chemical calculations. They compared the calculated binding energies with experimental values for some molecules and concluded that the calculated binding energies to one water molecule are proportional to the experimental values. However, it was also mentioned that this is only true if a covalent bond does not form between adsorbed species and the water molecule.

Consequently, estimating the binding energies of bare atomic radicals such as carbon, nitrogen, oxygen, and so on, is simply not doable by interpolating a one-water-molecule model into the experiments. In this work, we wish to propose a new calculation model to incorporate both statistical and quantum effects in the estimation of the binding energies of atoms and molecules to the amorphous solid water (ASW) surface, and to demonstrate our model for computing the binding energies of carbon (^3P), nitrogen (^4S), and oxygen (^3P).

In this paper, we first describe the computational model, which is applicable to estimating the binding energies of atoms and molecules in interstellar chemistry (Section 2). Next, we demonstrate our model for computing the binding energies of C, N, and O atoms on the ASW (Section 3). With these binding energies, we perform simulations based on the rate-equation method (Section 4.1) and discuss the impact on the chemical compositions of dense molecular clouds (Section 4.2). Finally, we close our discussions with concluding remarks and future perspectives (Section 5).

2. Computational Details

We present a new computational model of ASW to compute an adsorption energy; the model is simple yet able to take into account statistical features in interstellar environments. A key hypothesis is that an adsorbent will occupy the most stable site in a local region of ASW surface during a long time period, although motions of atoms and molecules are extremely slow because of the low-temperature conditions of the interstellar medium. In fact, the TPD experiments show that physisorbed species (at least for nonpolar molecules such as H_2, D_2, and N_2) are bound to deep potential sites on the ASW surface following diffusion, prior to thermal desorption (Kimmel et al. 2001; Hornekaer et al. 2005; Amiaud et al. 2006, 2007; Fillion et al. 2009). To capture these features in the adsorption energy calculation, we followed three steps when constructing our computational model: (1) several ASW clusters are generated from molecular dynamics (MD) annealing calculations, (2) the adsorbent is randomly added to each ASW cluster and optimizes the geometry using quantum chemistry calculations, and (3) the largest adsorption energies for each cluster are averaged, as shown schematically in Figure 1. All the MD calculations were performed using the Amber 14 program package (Kollman 2014) and all the quantum chemistry calculations were performed using the Gaussian 09 program package (Frisch 2015). In the following subsections, we will explain the details of each step.

2.1. An MD Annealing Simulation for Constructing Amorphous Solid Water (ASW) Clusters

First, we carried out MD annealing calculations using classical force fields to simulate a water cluster as a model of the ASW surface. We considered 20 water molecules with the TIP3P model and performed droplet simulations with a spherical constraint of 20 Å to prevent the escape of water molecules from the cluster. After 100 ps simulations at 300 K to achieve equilibrium, we took 11 different structures, each of which was annealed to 10 K, as initial guesses of quantum chemistry calculations. Next, these 11 different structures of water clusters were fully optimized on the basis of density functional theory (DFT) calculations using ω-B97XD functional (Chai & Head-Gordon 2008), in which the van der Waals (vdW) interaction is empirically incorporated. A valence triple-ζ plus polarization and diffuse functions, namely 6-311+G (d, p) basis sets, were adopted for both the geometry optimization and the adsorption energy evaluation. From these optimized structures, we discarded two structures because the annealing process failed to form a cluster. Consequently, we considered nine different structures of water clusters.

Due to the fluctuation of water molecules over a long time period, our scheme assumes that the ASW achieves a sort of equilibrium condition even in an extremely low-temperature environment. Sampling several cluster geometries captures different regions of the real ASW surface, therefore averaging the adsorption energies over clusters will be a good

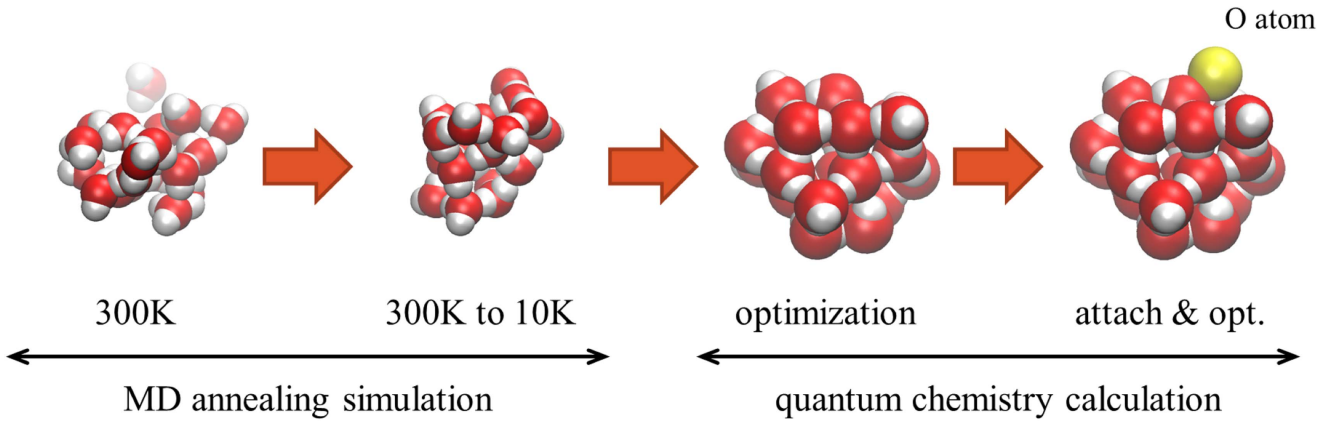

Figure 1. Computational steps for constructing an amorphous ice cluster model and its atom-adsorbed structure.

approximation of the average adsorption energy in the real ASW surface.

2.2. Adsorption Energy Evaluation

For nine selected structures of $[H_2O]_{20}$, we randomly added C, N, or O atoms around the surface area of the cluster and fully optimized the geometry using the same DFT functional and the same basis sets. We considered 10 different "trials" for 9 different "samples" of $[H_2O]_{20}$, therefore 90 different structures of the adsorbed clusters were examined. Finally, we chose the largest adsorption energies from 10 different trials and averaged them over 9 different samples to compute the adsorption energy. The largest adsorption energy from 10 different trials can capture the locally stable site at which the adsorbent resides for a long time period.

3. Calculated Adsorption Energies of C, N, and O Atoms to ASW

The calculated adsorption energies of carbon (^3P), nitrogen (^4S), and oxygen (^3P) to the $[H_2O]_{20}$ cluster are summarized in Table 1, in comparison to those from the previous experimental and computational results. Our results are qualitatively consistent with the adsorption energies estimated in Wakelam et al. (2017) using DFT/M06-2X calculations for the interaction of the species with one water molecule. In the following subsections, we discuss characteristic features of the adsorption for each atom according to calculated adsorption energy, geometry, and electronic structure.

Table 1
Calculated Adsorption Energy ($E_{ads.}$) of C, N, and O Atoms on the $[H_2O]_{20}$ Cluster

	C(^3P)	N(^4S)	O(^3P)
$E_{ads.}$	14,100	400	1440
Std. Error	420	30	160
Exptl.	N/A	720	1410
W17	10,000	1200	1700–2200

Note. Adsorption energies and standard errors are in units of Kelvin. Zero-point energy correction was incorporated. Experimentally observed adsorption energies of N and O atoms are shown in the third row (Minissale et al. 2016). Adsorption energies estimated in Wakelam et al. (2017) using DFT/M06-2X calculations are shown in the fourth row.

3.1. Carbon Atom

The most interesting finding in this work is that the adsorption of a C atom to ASW is classified as chemisorption; the adsorption energy was estimated to be 14,100 K (117 kJ mol^{-1}), which is apparently larger than that for common physisorption. In chemisorption, the carbon atom forms a chemical bond with an oxygen atom of water. Figure 2 shows histograms of the distances between the adsorbed C atom and the nearest-neighbor O and H atoms for 77 converged samples (R_{O-C} and R_{H-C}, respectively). Note that 13 samples were excluded, since geometry optimizations were not converged in 12 samples and chemical conversion occurs in the last sample. Interestingly, 80% of the samples took the R_{O-C} of less than 1.60 Å, which is only a little longer than the 1.43 Å of known aliphatic C–O bonds. This is further evidence that the adsorption of the C atom on the ASW surface is assigned as chemisorption. Furthermore, a somewhat broad peak for the R_{H-C} distribution is found in the range of 1.70–2.00 Å. Though this is apparently longer than the 1.08 Å of the typical C–H chemical bond length, this is considered a typical hydrogen bonding distance. Indeed, the O–H bond in which the nearest H atom to the adsorbed C atom is involved, favored the C atom. As a result, the adsorbed C atom is incorporated into the hydrogen bond network of the $[H_2O]_{20}$ cluster. Therefore, both the chemical interaction between the C and the O atoms and the hydrogen bonding interaction between the C and the H atoms contribute the large adsorption energy of the C atom. These are also shown by the correlation between the adsorption energy and either the R_{O-C} or the R_{H-C}; a shorter R_{O-C} or shorter R_{H-C} gives a larger adsorption energy (Figure 2).

The reaction of atomic carbon with water was experimentally suggested for gas-phase reactions in previous studies (e.g., Ahmed et al. 1983; Hickson et al. 2016). The formation of water-carbon adducts is also suggested for carbon atoms and water molecules in liquid helium droplets at ultra-low temperatures (~0.4 K, Krasnokutski & Huisken 2014). Previous quantum chemistry calculations supported the observed reactivity of atomic carbon with water (Ahmed et al. 1983; Ozkan & Dede 2012). Hickson et al. (2016) argued the importance of tunneling effects on the enhancement of the C+H_2O reaction at low temperatures. On the other hand, there are studies that report the non-reaction of carbon atoms with

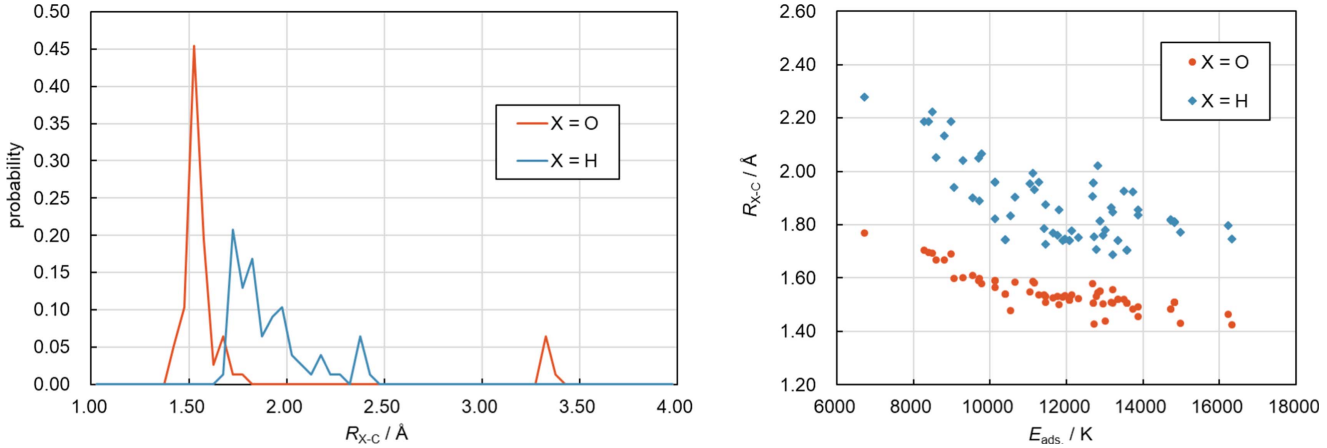

Figure 2. Left panel: histograms of distance between the adsorbed C atom and the nearest-neighbor atom (R_{X-C}, X = H and O). For every 0.05 Å, 77 converged samples were considered, and the frequency was divided by the number of samples. Right panel: correlation between the distance (R_{X-C}) and the adsorption energy of C atom ($E_{ads.}$).

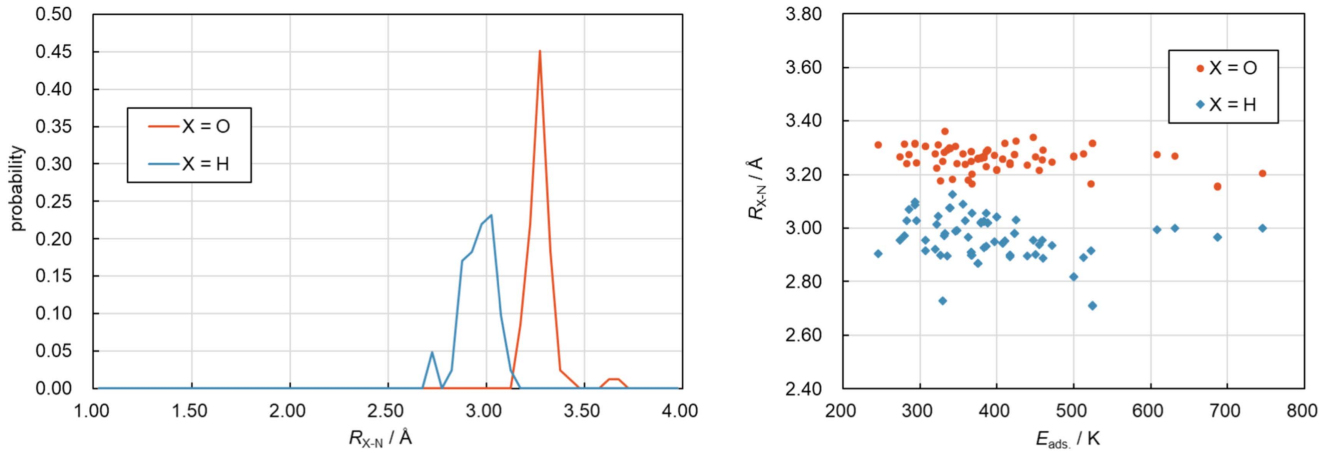

Figure 3. Left panel: histograms of distance between the adsorbed N atom and the nearest-neighbor atom (R_{X-N}, X = H and O). For every 0.05 Å, 82 converged samples were considered, and the frequency was divided by the number of samples. Right panel: correlation between the distance (R_{X-N}) and the adsorption energy of the N atom ($E_{ads.}$).

water in low-temperature (∼10 K) argon matrices (Ortman et al. 1990; Schreiner & Reisenauer 2006).

An impact of our results is that it is strongly suggested computationally that "chemical reaction occurs" between the C atom and a water molecule on the ASW surface upon adsorption, and it is of considerable importance for the chemical evolution of C–O species in interstellar space.

3.2. Nitrogen Atom

The adsorption energy of an N atom to the $[H_2O]_{20}$ cluster was estimated to be 400 K (3.33 kJ mol^{-1}), which is clearly classified as physisorption. The calculated adsorption energy of the N atom somewhat underestimated the experimental value (720 K). This underestimation would come from insufficient descriptions of the vdW interaction, as we have checked the adsorption energy of an N atom with the coupled-cluster calculation (CCSD(T) level of theory, which is known as a gold standard quantum chemistry method for common molecules) in a small model (see the Appendix). Consequently, we concluded that the DFT-computed adsorption energy is at least qualitatively correct. Figure 3 shows histograms of the distances between the adsorbed N atom and nearest-neighbor O and H atoms for 82 converged samples. Note that 8 samples were excluded because their geometry optimizations were not converged. From the histogram, a peak distribution of the N–O distance appears at R_{O-N} = 3.20–3.30 Å and that of the N–H distance appears at R_{H-N} = 2.85–3.00 Å. These trends can be explained in terms of vdW radii; estimated N–O and N–H distances are 3.07 Å and 2.75 Å, respectively (note that the vdW radii of 1.55 Å for N, 1.52 Å for O, and 1.20 Å for H are employed). Therefore, we concluded that the N atom adsorbs purely via the vdW interactions between the O and the H atoms of the water cluster.

Interestingly, neither the N–O distance nor the N–H distance correlate with the adsorption energy (Figure 3). This is because the adsorption energy mainly depends on the number of coordinate atoms around the adsorbed N atom.

3.3. Oxygen Atom

The adsorption energy of an O atom to the $[H_2O]_{20}$ cluster was computed to be 1440 K (12.0 kJ mol^{-1}), which is amazingly close to the experimentally reported value of 1410 K (Minissale et al. 2016). Consequently, our results systematically reproduced the adsorption energies of N and O atoms, at least qualitatively, and it is highly expected that the predicted adsorption energy of C atom is also reliable.

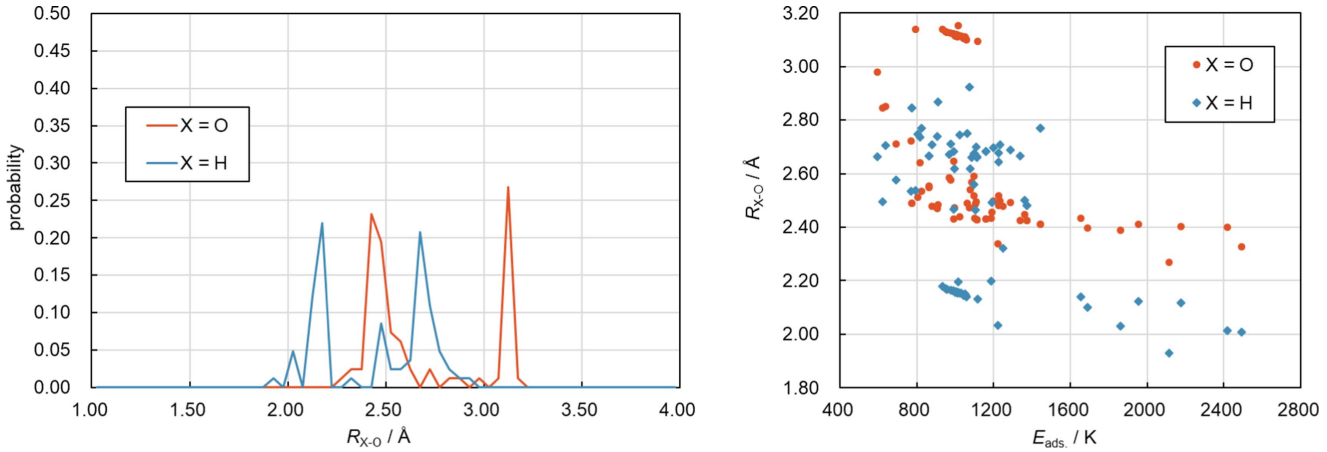

Figure 4. Left panel: histograms of distance between the adsorbed O atom and the nearest-neighbor atom ($R_{X–O}$, X = H and O). For every 0.05 Å, 82 converged samples were considered, and the frequency was divided by the number of samples. Right panel: correlation between the distance ($R_{X–O}$) and the adsorption energy of the O atom ($E_{ads.}$).

From the histogram of distances between the adsorbed O atom and the nearest-neighbor O and H atoms of the $[H_2O]_{20}$ cluster (Figure 4, left), there are two peaks for each $R_{O–O}$ or $R_{H–O}$ distribution. In the $R_{O–O}$ distribution, two peaks are found in the range of 2.40–2.50 Å and at 3.10 Å. In the $R_{H–O}$ distribution, two peaks are found in the range of 2.10–2.20 Å and in the range of 2.65–2.75 Å. According to vdW radii, the O–O and the H–O distances are estimated to be 3.04 Å and 2.72 Å, respectively, values that agree well with the second peaks of the $R_{O–O}$ and the $R_{H–O}$ distribution. On the other hand, the correlation between the distance ($R_{O–O}$ or $R_{H–O}$) and the adsorption energy is complex (Figure 4, right), so we are unable to understand the stability of the adsorbed structure. To make this clear, the correlation between the $R_{O–O}$ and the $R_{H–O}$ is investigated as shown in Figure 5. From these results, we found that there are three characteristic structures: (1) short $R_{O–O}$ and long $R_{H–O}$; (2) long $R_{O–O}$ and short $R_{H–O}$; and (3) short $R_{O–O}$ and short $R_{H–O}$. The long $R_{O–O}$ or the long $R_{H–O}$ distance is understood to mean that there is only the vdW interaction between the adsorbed O atom and the H_2O. A short $R_{O–O}$ or short $R_{H–O}$ distance implies that there is some sort of chemical bonding interaction, including the hydrogen bonding interaction; this is what we have seen in the adsorbed C atom, although these interactions are very weak compared to the C–O bonding interaction. Though structures (1) and (2) are associated with large probability, they are classified as meta-stable structures. Although structure (3) rarely occurs, it is stable in energy and in our estimation scheme, it is a large contributor to the adsorption energy of the O atom.

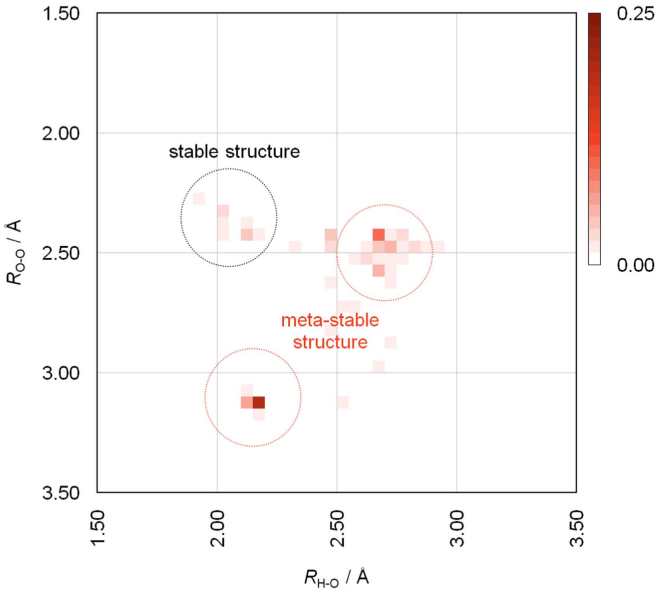

Figure 5. Correlation between the $R_{O–O}$ and the $R_{O–H}$ of the adsorbed O atom on $[H_2O]_{20}$.

4. Astrochemical Implications

4.1. Simulations of Dense Cloud Chemistry with the Rate-equation Method

We carried out gas-ice astrochemical simulations to examine the effect of the calculated adsorption energies on the chemical compositions of dense molecular clouds. We employed a pseudo-time-dependent gas-ice chemistry model, adopting the modified rate equation method (Hasegawa et al. 1992; Garrod 2008). The chemistry is described by a three-phase model (the gas phase, an icy grain surface, and the bulk ice mantle; Hasegawa & Herbst 1993). Our chemical network is originally based on that of Garrod & Herbst (2006), in which gas-phase reactions, interactions between gas and (icy) grain surfaces, and surface reactions are included. More details can be found in Furuya et al. (2016, 2017).

Simulations are performed for a static dense molecular cloud with a hydrogen nuclei density of $n_H = 2 \times 10^5$ cm^{-3} and a visual extinction of $A_V = 10$ mag. The temperatures of both gas and dust are fixed at 10 K or 15 K. A standard grain size of 0.1 μm in radius is assumed, with $\sim 10^6$ surface binding sites per grain and with a dust-to-gas mass ratio of 0.01. Initial gas-phase abundances are shown in Table 2 for important species; the initial species are assumed to be atoms or atomic ions, except for H_2 and CO. Almost all hydrogen is assumed to be in H_2, while half of carbon is assumed to be in CO.

Two sets of adsorption energies are investigated. Model 1 employs commonly used adsorption energies (C: 800 K, N: 800 K, O: 1600 K, e.g., Hama & Watanabe 2013), whereas Model 2 employs the adsorption energies that are calculated in this work (C: 14,100 K, N: 400 K, O: 1440 K, as in Table 1). The adsorption energy of atomic hydrogen is set to 350 K in both models. Note that our astrochemical models do not

Table 2
Initial Abundances of Selected Species

Species	Fractional Abundance w.r.t. n_H
H	5.0(−5)
H_2	5.0(−1)
C^+	4.0(−5)
N	2.5(−5)
O	1.4(−4)
CO	4.0(−5)

Note. $A(-B)$ means $A \times 10^{-B}$. Elemental abundances are taken from Aikawa & Herbst (1999).

consider the formation of a C–O bond upon adsorption of atomic carbon onto water ice for simplicity. The ratio of a diffusion energy relative to an adsorption energy is fixed to 0.6. The cosmic-ray ionization rate is set to 5.0×10^{-17} s^{-1} (Dalgarno 2006).

Note that adsorption energies of other species, particularly those of radicals, are important but uncertain parameters in astrochemical simulations, as pointed out in Wakelam et al. (2017). In the low-temperature regime that we consider in this work, the diffusion of such species is much less efficient compared to the formation of a monolayer ice (see Figure 6 and discussion in Section 4.2.2), because the adsorption energies of major radicals are generally believed to be higher than 1000 K (Wakelam et al. 2017, and references therein). We thus presume that uncertainties caused by diffusion of high-$E_{ads.}$ species would be moderated in the present simulations.

4.2. Implications for Ice Chemistry in Dense Molecular Clouds

Figures 7 and 8 show the results of gas-ice chemistry simulations at dust temperatures (T_{dust}) of 10 K and 15 K, respectively. Fractional abundances with respect to the total hydrogen nuclei density are compared between the model with commonly used adsorption energies (Model 1) and that with the newly calculated adsorption energies (Model 2). Abundances of selected species throughout the ice mantle extracted at 10^4, 10^5, and 10^6 yr are summarized in Tables 3–4. The following sections describe the effects of the modified adsorption energies on the abundances of carbon-, nitrogen-, and oxygen-bearing species in dense clouds.

4.2.1. Carbon-bearing Species

Most major carbon-bearing species are not significantly affected by the modification of adsorption energies, both at 10 K and 15 K (Figures 7(a), (b) and 8(a), (b)). One exception is atomic carbon ice, whose abundance decreases from Model 1 to Model 2 by about two orders of magnitude at 10 K. This would reflect the increased efficiency of the C+N reaction due to the increased surface mobility of atomic nitrogen. Note that the surface mobility of atomic hydrogen does not change between the two models because we use the same adsorption energy in both models.

On the other hand, at 15 K and in Model 1, the atomic carbon starts to diffuse on the grain surface to react with other species, which results in the decreased abundance of surface carbon atoms. However, this pathway is significantly suppressed in Model 2 because the increased adsorption energy of carbon makes the surface carbon atoms almost immobile, even at 15 K. Therefore, at 15 K, the abundance of atomic carbon ice

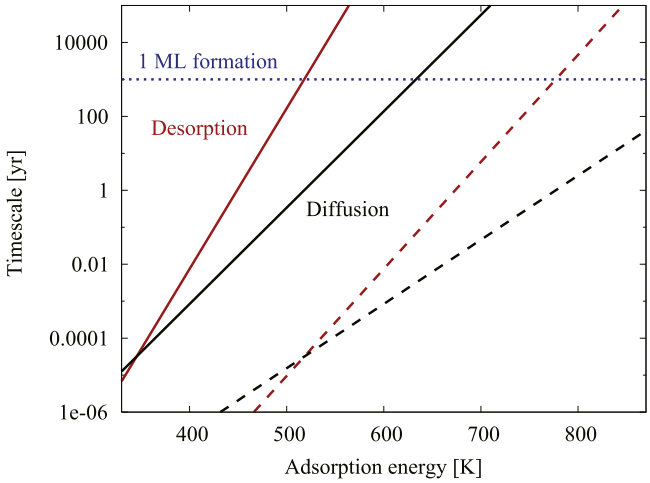

Figure 6. Timescales of the desorption (red), diffusion over 10^6 sites (black), and formation of a monolayer ice (blue dotted) as a function of adsorption energies. The solid lines represent the case of 10 K, while the dashed lines represent that of 15 K. A lower adsorption energy leads to more efficient surface diffusion, which increases the chance of meeting the reaction partner before being locked into the ice mantle. The characteristic frequency for diffusion and desorption is assumed to be 10^{12} s^{-1}. The gas density is assumed to be 2×10^5 cm^{-3}. See Section 4.2.2 for more details.

is higher in Model 2 than in Model 1. The high adsorption energy of carbon implies that its surface diffusion is less efficient until the self-diffusion of water molecules starts at an elevated temperature (∼90 K, Ghesquière et al. 2015).

The chemisorption of carbon atom on water ice, suggested in our quantum chemistry calculation, implies the possibility of further chemical reactions producing molecules bearing a C–O bond such as formaldehyde (H_2CO) or methanol (CH_3OH), though it may hinder the formation of methane (CH_4) on water ice via sequential hydrogenation of carbon atoms. Although this would have a large impact on the chemical evolution of carbon-bearing species, the present astrochemical model does not include these reaction pathways, due to the lack of available chemical network information. Further efforts to involve those reactions will be important future works.

Furthermore, the decreased mobility of atomic carbon would affect the efficiency of organic chemistry that is triggered by the surface diffusion of carbon atoms. Several chemical pathways leading to the formation of complex organic molecules through addition reactions of atomic carbon and hydrogen to CO are suggested in the literature (e.g., Figure 12 in Herbst & van Dishoeck 2009, and references therein). The present results imply that these pathways, which require the diffusion of atomic carbon (or hydrogenated products of CO), would be less efficient in actual molecular cloud conditions than had been previously thought, due to the decreased mobility of surface carbon atoms.

4.2.2. Nitrogen-bearing Species

Nitrogen-bearing species are significantly affected by the present modification of adsorption energies. At 10 K and in Model 1, the most abundant nitrogen-bearing species is NH_3, because hydrogenation dominates grain surface reactions (Figure 7(c)). In Model 2, however, N_2 takes the place of the major nitrogen reservoir, because the decreased adsorption energy of atomic nitrogen leads to effective diffusion, which results in a competition between hydrogenation and

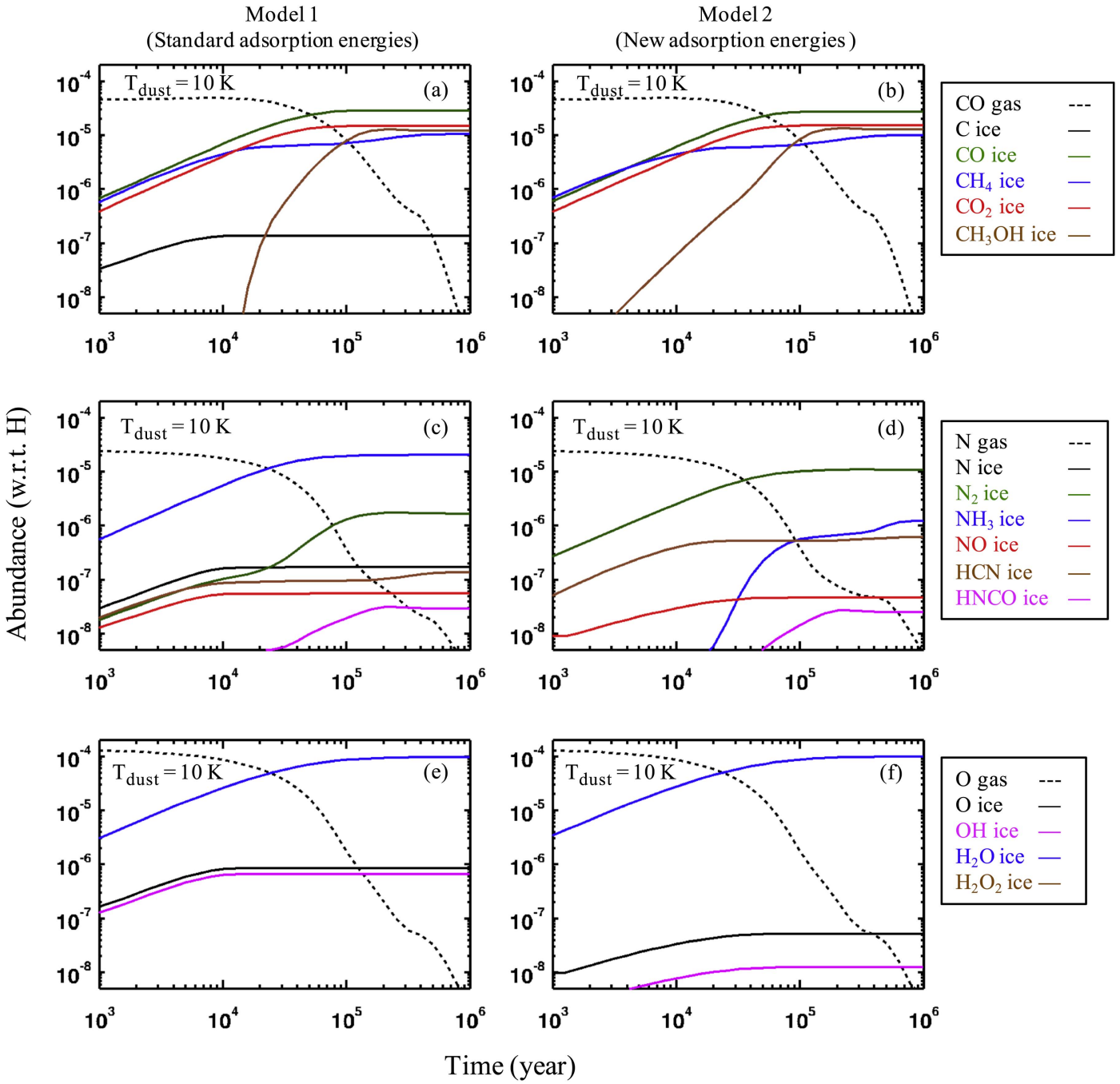

Figure 7. Chemical compositions of a dense molecular cloud (T_{dust} = 10 K) calculated by the rate equation method using two different sets of adsorption energies; Model 1 (left) and Model 2 (right) (see Section 4.1). Time-dependent fractional abundances of important surface species are shown by solid lines in each panel; (a) and (b) are carbon-bearing species, (c) and (d) are nitrogen-bearing species, and (e) and (f) are oxygen-bearing species. The abundances of major gas-phase species (CO, N, O) are shown by dashed lines.

nitrogenation (Figure 7(d)). In addition, as a consequence of the increased surface reactivity of nitrogen atoms, the abundance of the N ice decreases in Model 2 by nearly seven orders of magnitude compared to Model 1. A slight increase of HCN in Model 2 is also seen.

Figures 6 shows timescales of the surface diffusion (scanning of 10^6 sites), desorption, and formation of a single ice layer as a function of the adsorption energy of a surface species. We use the inverse of Equation (4) and (12) in Cuppen et al. (2017) to calculate the plotted timescales. The figure indicates that, at 10 K and with $E_{ads.}$ = 800 K, both diffusion and desorption are much slower than the formation of a monolayer, thus surface species will hardly have the chance to find a reaction partner before being embedded in the mantle phase. On the other hand, with $E_{ads.}$ = 400 K, the diffusion is much faster than the layer formation and thus surface species have a sufficient chance to meet the reaction partner. At 15 K, surface species can diffuse rapidly enough to react before the formation of another ice layer, even with $E_{ads.}$ = 800 K, thanks to the elevated temperature.

An enhancement of surface nitrogenation that is caused by the efficient diffusion of nitrogen atoms has important

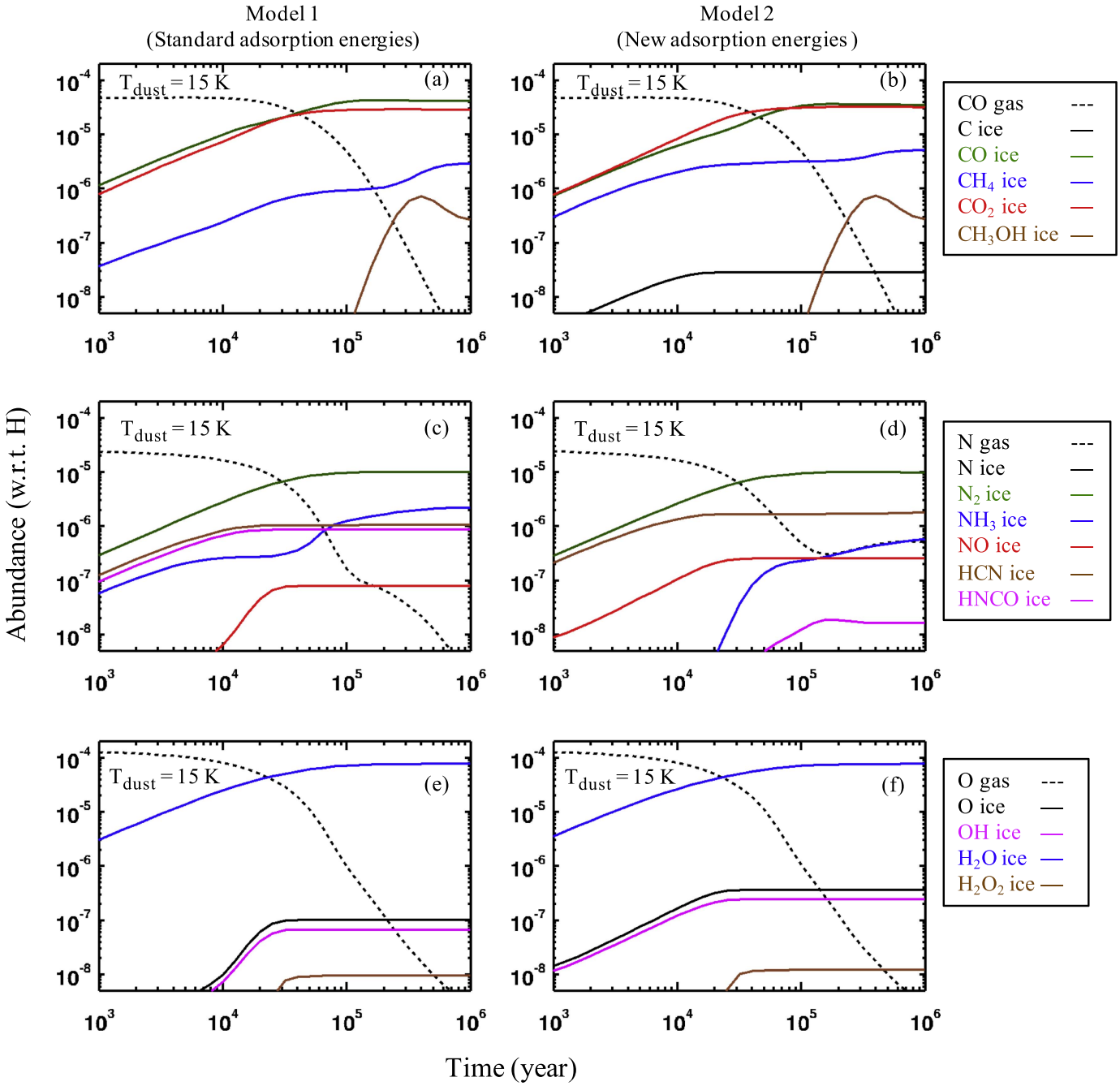

Figure 8. Same as Figure 7 but for T_{dust} = 15 K.

astrochemical implications. So far, N_2 ice has not been detected directly in dense molecular clouds due to the lack of strong infrared bands (e.g., Sandford et al. 2001). The suggested formation of N_2 as a main reservoir of nitrogen in a dark cloud environment therefore has important theoretical implications for the nitrogen budget in dense molecular clouds. The universality of the efficient N_2 formation, however, should be further investigated for more diverse interstellar conditions.

In general, published gas-ice astrochemical models of dense molecular clouds overestimate the NH_3/H_2O abundance ratio by a factor of a few (e.g., Vasyunin & Herbst 2013; Chang & Herbst 2014; Furuya et al. 2015), compared to the observationally derived abundance ratio in dense clouds (e.g., Dartois & d'Hendecourt 2001; Gibb et al. 2001; Dartois et al. 2002; Bottinelli et al. 2010). The decreased NH_3 abundance with respect to H_2O ice in Model 2 is consistent with the ice observations. Figure 9 shows the calculated NH_3 abundances as a function of the adopted adsorption energies of atomic nitrogen. Observed abundances of the NH_3 ice toward low-mass and high-mass protostars are also shown for comparison purposes. It is shown that high nitrogen adsorption energies such as those in Model 1 overproduce NH_3, compared to the observations, while low adsorption energies, such as those in our quantum chemistry calculations, better reproduce the observed NH_3 ice abundances. Note that the nitrogen adsorption energy of 400 K in Model 2 may underproduce NH_3 to some degree, compared to the observations, since the calculated NH_3 abundance is located at the lower end of the

Table 3
Abundances of Species throughout the Ice Mantle for 10 K Dust

Species	Model 1[a]			Model 2[b]		
	10^4 years	10^5 years	10^6 years	10^4 years	10^5 years	10^6 years
C	1.4(−7)	1.4(−7)	1.4(−7)	2.6(−9)	2.8(−9)	2.8(−9)
CO	7.0(−6)	2.9(−5)	2.9(−5)	6.2(−6)	2.7(−5)	2.7(−5)
CH_4	4.6(−6)	7.2(−6)	1.1(−5)	4.6(−6)	6.8(−6)	1.0(−5)
CO_2	4.1(−6)	1.5(−5)	1.5(−5)	4.0(−6)	1.5(−5)	1.5(−5)
CH_3OH	1.2(−10)	8.0(−6)	1.2(−5)	6.3(−8)	8.7(−6)	1.3(−5)
N	1.6(−7)	1.7(−7)	1.7(−7)	5.6(−15)	2.9(−14)	3.1(−14)
N_2	1.0(−7)	1.3(−6)	1.7(−6)	2.6(−6)	1.0(−5)	1.1(−5)
NH_3	5.6(−6)	2.0(−5)	2.1(−5)	1.7(−9)	5.7(−7)	1.3(−6)
NO	5.4(−8)	5.6(−8)	5.6(−8)	3.0(−8)	4.7(−8)	4.7(−8)
HCN	8.7(−8)	9.6(−8)	1.4(−7)	4.1(−7)	5.3(−7)	6.2(−7)
HNCO	4.6(−9)	2.0(−8)	2.9(−8)	1.0(−10)	1.4(−8)	2.5(−8)
O	8.3(−7)	8.6(−7)	8.6(−7)	3.4(−8)	5.2(−8)	5.2(−8)
O_2	8.9(−11)	5.7(−10)	5.8(−10)	4.7(−12)	5.9(−10)	6.0(−10)
OH	6.5(−7)	6.7(−7)	6.7(−7)	7.9(−9)	1.3(−8)	1.3(−8)
H_2O	2.6(−5)	8.7(−5)	9.7(−5)	2.8(−5)	8.8(−5)	9.9(−5)
H_2O_2	1.6(−10)	1.1(−9)	1.1(−9)	7.8(−12)	1.0(−9)	1.0(−9)

Notes. $A(-B)$ means $A \times 10^{-B}$.
[a] Standard adsorption energies.
[b] New adsorption energies calculated in this work. See Section 4.1 for details on the adsorption energies used in each model.

observed abundance range. This would suggest that the actual adsorption energy of atomic nitrogen might be somewhat higher than the present result, as also mentioned in Section 3.2.

At 15 K, the dominant nitrogen reservoir is N_2 both in Model 1 and 2 because the surface mobility of atomic nitrogen increases at a higher dust temperature (Figures 8(c), (d)). At this temperature, the effect of the modified adsorption energies appears as the decreased abundances of NH_3 and HNCO, and the increased abundances of HCN and NO. A possible explanation of the behaviors of NH_3 and HCN is the same as in the case of the 10 K simulation described above. The slight increase of NO is possibly due to the decreased destruction via NO + C → OCN, which is caused by the increased adsorption energy of carbon in Model 2. Accordingly, the reduced formation of OCN results in the decrease of HNCO, which is formed by OCN+H in our chemical model.

4.2.3. Oxygen-bearing Species

The most abundant oxygen-bearing species, H_2O, is affected little by the modification of adsorption energies both at 10 K and 15 K (Figures 7(e), (f) and 8(e), (f)). The behaviors of relatively minor solid species, O and OH, are rather complicated; their abundances decrease from Model 1 to Model 2 at 10 K, while they increase from Model 1 to Model 2 at 15 K. Because the oxygen adsorption energies used in Model 1 and Model 2 are close, the abundance differences seen in those oxygen-bearing species are likely due to the indirect effect caused by modifications of the carbon and nitrogen adsorption energies. The decrease of O and OH from Model 1 to Model 2 at 10 K may be due to the enhancement of the N+O reaction in Model 2, while the increase of O and OH from Model 1 to Model 2 at 15 K may reflect the suppression of O production by the diffusive surface reaction of carbon- and oxygen-bearing species. Note that the O_2 ice is not shown in the figures because its abundance is always lower than 10^{-8} in our calculation (Tables 3–4).

5. Conclusions

We carried out quantum chemistry calculations to estimate the adsorption energies of atomic carbon, nitrogen, and oxygen on the low-temperature amorphous water ice surface. In addition, we investigate the effect of newly calculated adsorption energies on the chemical compositions of dense molecular clouds with the aid of a gas-ice astrochemistry simulation. We obtain the following conclusions:

1. A new computational model that is able to merge quantum chemical and statistical contributions to binding energies of atoms and molecules in interstellar chemistry is proposed. The basis of our computational model is that an atom or a molecule adsorbs to the most stable local site on the ASW surface over a long period of time. This is achieved by considering variations of adsorption sites on ASW by sampling structures of water clusters. Therefore, it is advantageous that quantum chemical calculations are available in our computational model, because only small computational efforts are required to evaluate statistical effects. Although our computational results might not be converged from a statistical viewpoint because we only sampled a small number of water clusters for demonstration, we conclude that our model is quite useful to theoretically estimate binding energies in interstellar chemistry.
2. The calculated adsorption energies of atoms on ASW are 14,100 ± 420 K for carbon, 400 ± 30 K for nitrogen, and 1440 ± 160 K for oxygen. The estimated binding energy of oxygen agrees well with the experimental numbers. An N atom takes pure physisorption, therefore the binding energy of an N atom is amazingly small. On the other hand, a C atom undergoes chemisorption to form a chemical bond with an O atom in a water molecule. An O atom has a dual character and experiences both physisorption and chemisorption.

Table 4
Abundances of Species throughout the Ice Mantle for 15 K Dust

Species	Model 1[a]			Model 2[b]		
	10^4 years	10^5 years	10^6 years	10^4 years	10^5 years	10^6 years
C	3.6(−11)	3.7(−11)	3.7(−11)	2.3(−8)	2.9(−8)	2.9(−8)
CO	1.0(−5)	4.0(−5)	4.2(−5)	6.2(−6)	3.4(−5)	3.5(−5)
CH_4	2.5(−7)	9.5(−7)	3.0(−6)	2.1(−6)	3.2(−6)	5.2(−6)
CO_2	7.5(−6)	2.8(−5)	2.9(−5)	8.5(−6)	3.2(−5)	3.2(−5)
CH_3OH	2.2(−12)	1.9(−9)	2.7(−7)	5.2(−12)	2.3(−9)	2.7(−7)
N	6.6(−11)	9.0(−11)	9.0(−11)	5.7(−19)	5.3(−18)	6.0(−18)
N_2	2.8(−6)	9.8(−6)	1.0(−5)	2.7(−6)	9.5(−6)	9.9(−6)
NH_3	2.6(−7)	1.3(−6)	2.2(−6)	8.4(−10)	2.3(−7)	6.0(−7)
NO	6.6(−9)	8.0(−8)	8.0(−8)	1.1(−7)	2.5(−7)	2.5(−7)
HCN	8.4(−7)	1.0(−6)	1.1(−6)	1.4(−6)	1.7(−6)	1.8(−6)
HNCO	6.8(−7)	8.8(−7)	8.8(−7)	1.2(−10)	1.3(−8)	1.6(−8)
O	1.0(−8)	1.0(−7)	1.0(−7)	1.7(−7)	3.7(−7)	3.7(−7)
O_2	4.9(−12)	2.8(−9)	2.8(−9)	4.2(−11)	3.7(−9)	3.7(−9)
OH	7.4(−9)	6.7(−8)	6.7(−8)	1.2(−7)	2.5(−7)	2.5(−7)
H_2O	2.5(−5)	7.2(−5)	7.8(−5)	2.7(−5)	7.1(−5)	7.7(−5)
H_2O_2	1.7(−11)	9.6(−9)	9.6(−9)	1.4(−10)	1.2(−8)	1.2(−8)

Notes. $A(-B)$ means $A \times 10^{-B}$.
[a] Standard adsorption energies.
[b] New adsorption energies calculated in this work. See Section 4.1 for details on the adsorption energies used in each model.

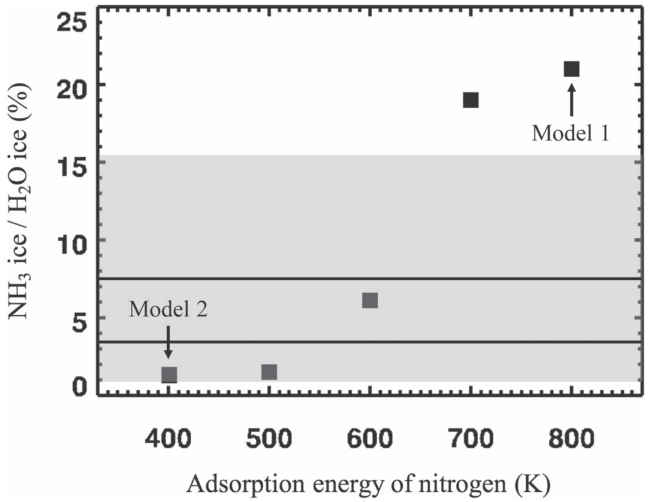

Figure 9. Calculated NH_3 ice abundances (T_{dust} = 10 K and time = 10^6 year) as a function of the adopted nitrogen adsorption energies (filled squares). The shaded area represents the range of the observed NH_3 ice abundances toward low-mass and high-mass protostars (Dartois & d'Hendecourt 2001; Gibb et al. 2001; Dartois et al. 2002; Bottinelli et al. 2010). The two solid lines represent the range of an average and a standard deviation of the NH_3 ice abundances for low-mass protostars (5.5 ± 2.0% as reported in Bottinelli et al. 2010). The adsorption energies of atomic nitrogen used in Model 1 and Model 2 are labeled.

Consequently, the binding energies are of the order C ≫ O > N.

3. The high adsorption energy of carbon suggests that its surface diffusion is less efficient until water molecules start to diffuse at high temperatures. This decreased mobility of carbon would suppress the previously suggested formation pathways of complex organic molecules, which are triggered by the surface diffusion of atomic carbon. On the other hand, the chemisorption of the C atom also suggests the possibility of further chemical reactions producing molecules bearing a C–O bond, such as formaldehyde, methanol, and so on. This would have a large impact on our knowledge of the chemical evolution of carbon-bearing species in dense molecular clouds, and we are going to extend our model to involve such reactions in astrochemical simulations in a future work.
4. The low adsorption energy of nitrogen implies that atomic nitrogen can efficiently diffuse on the surface even at 10 K. This significantly alters the chemical compositions of nitrogen-bearing molecules in dense molecular clouds. The most notable effect is that the N_2 is formed as a main reservoir of nitrogen instead of NH_3 at low temperatures, because surface nitrogenation competes with hydrogenation.
5. Major oxygen-bearing surface species are little affected by the application of the new adsorption energies.

Future works will need to investigate the adsorption energies of additional atoms and molecules of astrochemical interest.

This work is supported by a Grant-in-Aid from the Japan Society for the Promotion of Science (15K17612), and Building of Consortia for the Development of Human Resources in Science and Technology, MEXT, Japan. The authors are grateful to Prof. Yuri Aikawa and Prof. Naoki Watanabe for fruitful discussions and helpful suggestions. Finally, we would like to thank an anonymous referee for the careful reading and helpful comments.

Software: Amber 14 (Kollman 2014), Gaussian 09 (Frisch 2015).

Appendix
Adsorption Energies of C, N, and O Atoms Estimated by Different Calculation Methods

Table 5 summarizes the adsorption energies of carbon, nitrogen, and oxygen atoms to one water molecule as estimated by three different calculation methods. See the discussion in Section 3.2.

Table 5
Adsorption Energies of C, N, and O Atoms to One Water Molecule, Estimated Using DFT (ωB97XD/6-311+G(d, p)), MP2/aug-cc-pVQZ, and CCSD(T)/aug-cc-pVQZ Levels of Theory

Species	Adsorption Energy (K)		
	ωB97XD	MP2	CCSD(T)[a]
C–OH_2	5708	4289	4314
C–HOH	497	594	605
N–OH_2	Not bound	105	124
N–HOH	131	163	183
O–OH_2	926	473	528
O–HOH	823	842	879

Note. Species "XOH_2" and "XHOH" (X = C, N, and O) denote whether X atom binds to an O or H atom of the water molecule.
[a] CCSD(T) calculations were carried out based on the MP2-optimized geometry.

ORCID iDs

Takashi Shimonishi https://orcid.org/0000-0002-0095-3624
Kenji Furuya https://orcid.org/0000-0002-2026-8157

References

Ahmed, S. N., McKee, M. L., & Shevlin, P. B. 1983, JAChS, 105, 3942
Aikawa, Y., & Herbst, E. 1999, ApJ, 526, 314
Al-Halabi, A., Kleyn, A., Van Dishoeck, E., & Kroes, G. 2002, JPCB, 106, 6515
Al-Halabi, A., & van Dishoeck, E. F. 2007, MNRAS, 382, 1648
Amiaud, L., Dulieu, F., Fillion, J.-H., Momeni, A., & Lemaire, J. 2007, JChPh, 127, 144709
Amiaud, L., Fillion, J., Baouche, S., et al. 2006, JChPh, 124, 094702
Ásgeirsson, V., Jónsson, H., & Wikfeldt, K. 2017, The Journal of Physical Chemistry C, 121, 1648
Bottinelli, S., Boogert, A. C. A., Bouwman, J., et al. 2010, ApJ, 718, 1100
Buch, V., & Czerminski, R. 1991, JChPh, 95, 6026
Burke, D. J., & Brown, W. A. 2010, PCCP, 12, 5947
Chai, J.-D., & Head-Gordon, M. 2008, PCCP, 10, 6615
Chang, Q., & Herbst, E. 2014, ApJ, 787, 135
Cuppen, H. M., Walsh, C., Lamberts, T., et al. 2017, SSRv, 212, 1
Dalgarno, A. 2006, PNAS, 103, 12269
Dartois, E., & d'Hendecourt, L. 2001, A&A, 365, 144
Dartois, E., d'Hendecourt, L., Thi, W., Pontoppidan, K. M., & van Dishoeck, E. F. 2002, A&A, 394, 1057
Dupuy, J. L., Lewis, S. P., & Stancil, P. C. 2016, ApJ, 831, 54
Fillion, J.-H., Amiaud, L., Congiu, E., et al. 2009, PCCP, 11, 4396
Frisch, M. J. 2015, Gaussian, 09, http://Gaussian.com/
Furuya, K., Aikawa, Y., Hincelin, U., et al. 2015, A&A, 584, A124
Furuya, K., Drozdovskaya, M. N., Visser, R., et al. 2017, A&A, 599, A40
Furuya, K., van Dishoeck, E. F., & Aikawa, Y. 2016, A&A, 586, A127
Garrod, R. T. 2008, A&A, 491, 239
Garrod, R. T., & Herbst, E. 2006, A&A, 457, 927
Ghesquière, P., Mineva, T., Talbi, D., et al. 2015, PCCP, 17, 11455
Gibb, E. L., Whittet, D. C. B., & Chiar, J. E. 2001, ApJ, 558, 702
Hama, T., Kuwahata, K., Watanabe, N., et al. 2012, ApJ, 757, 185
Hama, T., & Watanabe, N. 2013, ChRv, 113, 8783
Hasegawa, T. I., & Herbst, E. 1993, MNRAS, 263, 589
Hasegawa, T. I., Herbst, E., & Leung, C. M. 1992, ApJS, 82, 167
He, J., Shi, J., Hopkins, T., Vidali, G., & Kaufman, M. J. 2015, ApJ, 801, 120
Herbst, E., & van Dishoeck, E. F. 2009, ARA&A, 47, 427
Hickson, K. M., Loison, J.-C., Nuñez-Reyes, D., & Méreau, R. 2016, The Journal of Physical Chemistry Letters, 7, 3641
Hornekær, L., Baurichter, A., Petrunin, V., et al. 2005, JChPh, 122, 124701
Hornekær, L., Baurichter, A., Petrunin, V., Field, D., & Luntz, A. 2003, Sci, 302, 1943
Karssemeijer, L. J., & Cuppen, H. M. 2014, A&A, 569, A107
Kimber, H. J., Ennis, C. P., & Price, S. D. 2014, FaDi, 168, 167
Kimmel, G. A., Stevenson, K. P., Dohnalek, Z., Smith, R. S., & Kay, B. D. 2001, JChPh, 114, 5284
Kollman, P. A. 2014, AMBER, 14, http://ambermd.org/
Krasnokutski, S. A., & Huisken, F. 2014, JChPh, 141, 214306
Kuwahata, K., Hama, T., Kouchi, A., & Watanabe, N. 2015, PhRvL, 115, 133201
Lee, M. W., & Meuwly, M. 2014, FaDi, 168, 205
Manicò, G., Ragunì, G., Pirronello, V., Roser, J. E., & Vidali, G. 2001, ApJL, 548, L253
Matar, E., Congiu, E., Dulieu, F., Momeni, A., & Lemaire, J. L. 2008, A&A, 492, L17
Medveď, I., & Černỳ, R. 2011, Microporous and Mesoporous Materials, 142, 405
Minissale, M., Congiu, E., & Dulieu, F. 2016, A&A, 585, A146
Ortman, B. J., Hauge, R. H., Margrave, J. L., & Kafafi, Z. H. 1990, JPhCh, 94, 7973
Ozkan, I., & Dede, Y. 2012, IJQC, 112, 1165
Penteado, E. M., Walsh, C., & Cuppen, H. M. 2017, ApJ, 844, 71
Perets, H. B., Biham, O., Manicó, G., et al. 2005, ApJ, 627, 850
Pirronello, V., Manicó, G., Roser, J., & Vidali, G. 2004, in ASP Conf. Ser. 309, Astrophysics of Dust, ed. A. N. Witt, G. C. Clayton, & B. T. Draine (San Francisco, CA: ASP), 529
Sandford, S. A., Bernstein, M. P., Allamandola, L. J., Goorvitch, D., & Teixeira, T. C. V. S. 2001, ApJ, 548, 836
Schreiner, P. R., & Reisenauer, H. P. 2006, ChemPhysChem, 7, 880
Senevirathne, B., Andersson, S., Dulieu, F., & Nyman, G. 2017, MolAs, 6, 59
Sladek, K. J., Gilliland, E. R., & Baddour, R. F. 1974, Industrial & Engineering Chemistry Fundamentals, 13, 100
Tielens, A. G. G. M., & Hagen, W. 1982, A&A, 114, 245
Vasyunin, A. I., & Herbst, E. 2013, ApJ, 762, 86
Veeraghattam, V. K., Manrodt, K., Lewis, S. P., & Stancil, P. C. 2014, ApJ, 790, 4
Vidali, G., Roser, J. E., Ling, L., et al. 2006, FaDi, 133, 125
Wakelam, V., Loison, J.-C., Mereau, R., & Ruaud, M. 2017, MolAs, 6, 22
Ward, M. D., Hogg, I. A., & Price, S. D. 2012, MNRAS, 425, 1264
Watanabe, N., Kimura, Y., Kouchi, A., et al. 2010, ApJL, 714, L233